Oxygen vacancies in a La0.5Sr2.5M2O7 compositionally complex perovskite

Neutron Physics Laboratory - Neutron diffraction

Rebecca Clulow

Proposal ID

588

Report regarding proposal "Oxygen vacancies in a $La_{0.5}Sr_{2.5}M_2O_{7-\delta}$ compositionally complex perovskite"

R. Clulow Uppsala University, Sweden

Compositionally complex perovskites are a new and promising area of research, the compounds contain multiple principle elements in near equimolar amounts which gives rise to vast chemical flexibility and tuneable properties. One application for this class of materials is as proton conducting materials for Solid Oxide Fuel Cells (SOFCs). SOFCs offer a route to convert chemical energy to electrical energy with greater efficiency and fewer emissions that other methods, however, their use is currently limited by their high operating temperatures.[1] Proton conducting fuel cells could provide a solution but new materials which balance good stability and high conductivity are still needed. Compositionally complex perovskites are candidates for solid oxide fuel cells since the highly disordered nature of the cations will avoid vacancy pinning whilst the highly tuneable nature will allow for control over the thermal expansion of the material – two of the current issue for SOFCs materials.[2]

The current study investigates the compositionally complex $La_{3-x}Sr_xM_2O_{7-\delta}$ n = 2 Ruddlesden-Poppers where M = Ti, Mn, Fe, Co, Ni. The structure and purity of the compound has previously been studied using X-ray diffraction at room temperature. The compound adopts the I4/mmm space group with unit cell parameters of a = 3.8551(1) and c = 20.1646(4) Å. Based upon the typical oxidation states of the cations present, the compound should contain oxygen vacancies for charge balance.

The aim of the experiment was to investigate the crystal structure, specifically the location and ordering of any oxygen vacancies. The presence and ordering of the oxygen vacancies within the compounds would be critical to the ionic conductivity of the material. The results of the preliminary refinement are shown below. The data are consistent with the *I*4/*mmm* model identified during the in-house X-ray diffraction measurements with no evidence of long-range cation ordering. The refined oxygen occupancies revealed an oxygen deficient 2*a* site with an occupancy of 0.78(3). The results will be combined with EDS and X-ray data before being published in a manuscript concerning the synthesis of compositionally complex n = 2 Ruddlesden-Popper perovskites.

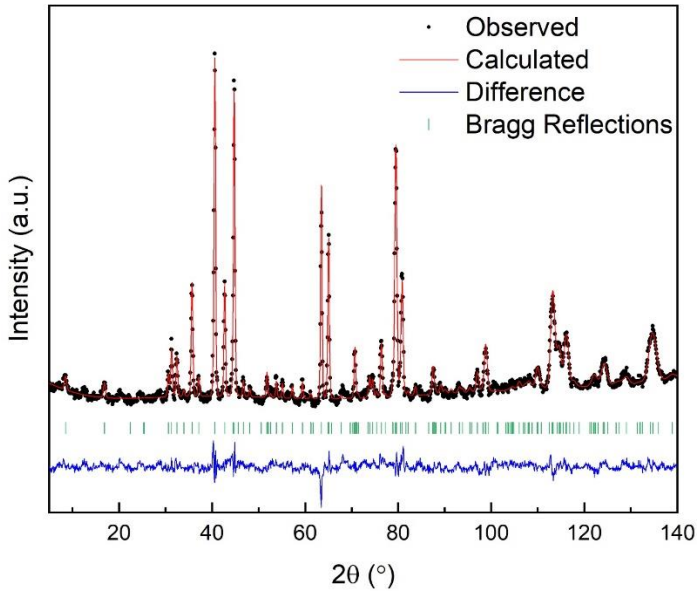

Figure 1: Powder neutron diffraction pattern and Rietveld refinement of $La_{0.5}Sr_{2.5}(TiMnFeCoNi)_2O_{7-\delta}$ R_{wp} 5.04 χ^2 3.44. Refined unit cell parameters a = 3.8507(2) and c = 20.1348(14) Å.

References

1 L. Fan, B. Zhu, P. C. Su and C. He, *Nano Energy*, 2018, **45**, 148–176.

2 A. J. Jacobson, *Chem. Mater.*, 2010, **22**, 660–674.

Characterisation of glass tesserae from unique mediaeval statue of Madonna in Malbork (PL)

Laboratory of Tandetron

Zdeka ermáková

Proposal ID

560

Report regarding proposal “Characterisation of glass tesserae from unique mediaeval statue of Madonna in Malbork (PL)”

Z. Čermáková, S. Švarcová, Institute of Inorganic Chemistry of CAS, v.v.i., Řež, Czech Republic

V. Havránek, Nuclear Physics Insitute of CAS, v.v.i., Řež, Czech Republic

Malbork Madonna is a unique mediaeval statue (destroyed at the end of World War II, but re-erected during recent restoration campaign with newly-made glass tesserae). The subject of this PIXE study were three types of preserved tesserae with special focus on a blue tessera, which was suspected to be original mediaeval. The measurements yielded elemental maps (Fig. 1), however, elements present at low concentration (see Sr) were very difficult to detect, and the obtained results were comparable with maps previously achieved by SEM-EDS.

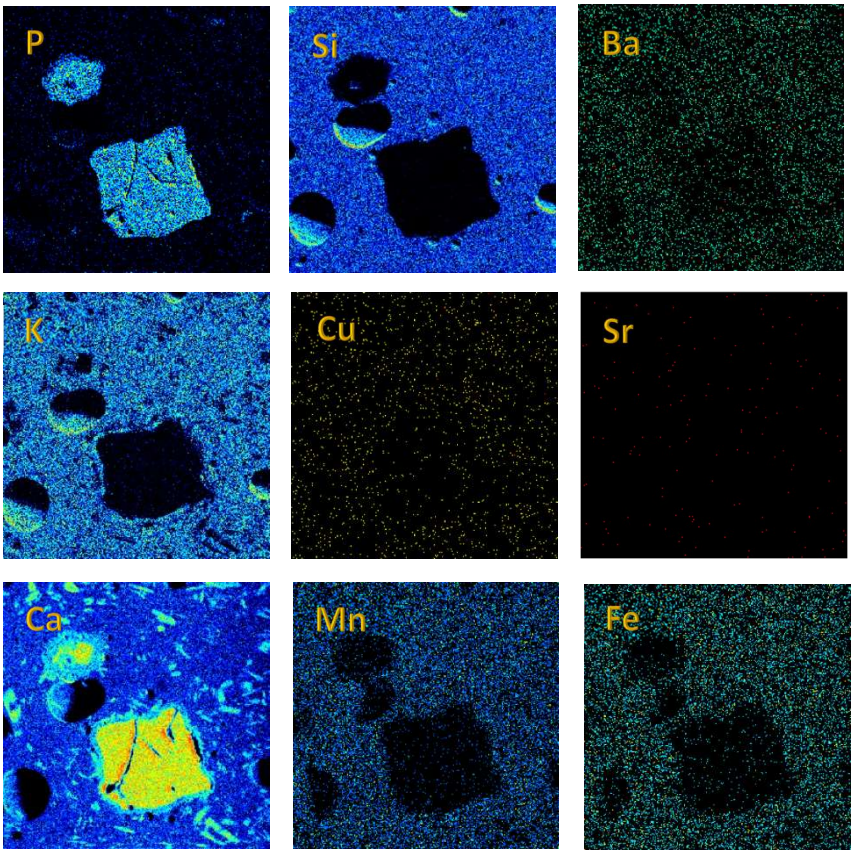

Fig. 1 PIXE elemental maps of the blue Malbork tessera with visible angular grains of Ca-phosphate and smaller inclusions of wollastonite/pseudowollastonite (phases identified by Raman microspectroscopy)

The calculations yielded some interesting results, such as confirmation of presence of Ba, or the detection of Ni, Cu or Zn, however, the analysis (especially if smaller areas were intended for future measurements) does not seem suitable for our purposes and it will be more meaningful to measure the samples by LA-ICP-MS, even though micro-destructive.

Diffusion of oxygen into a polymer-like film

Laboratory of Tandetron

Vladimir Cech

Proposal ID

595

Report on the proposal “Diffusion of oxygen into a polymer-like film”

Vladimir Cech, Brno University of Technology, Brno, Czech Republic
Oleksandr Romanenko, Anna Macková, Nuclear Physics Institute, Rez, Czech Republic

Nonthermal plasma-deposited sandwich structures consisting of glassy silica and a polymer layer in various orders were covered with an ultrathin barrier coating of silicon carbide to prevent the diffusion of atmospheric oxygen and water molecules into the polymer material.

Fresh and aged sandwich structures (Fig. 1) were analyzed using RBS / ERDA techniques to determine the possible oxidation of the polymer material. The simulated data required the addition of a thin interlayer between the oxide and polymer layers at the expense of the polymer layer thickness to fit the experimental data (Fig. 2).

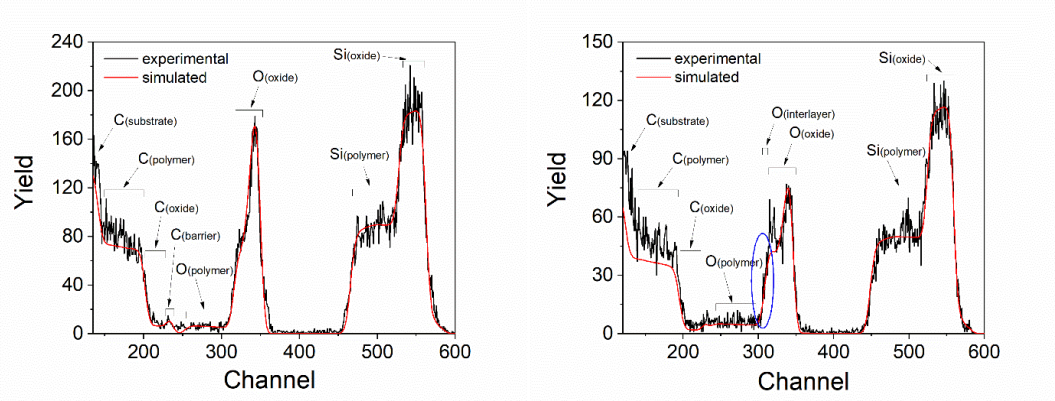

Fig. 1. RBS spectra of (a) 45 days and (b) 831 days stored sandwich structure.

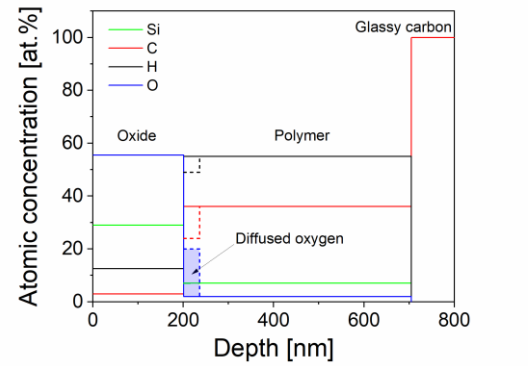

Fig. 2. Elemental depth profile of as-deposited (solid line) and aged (dashed line) sandwich structure. Diffused oxygen is indicated by the blue area.

This study revealed that glassy silica is a slightly porous material (3 vol.%) with small pores (2.5 nm) formed during thin film deposition and containing gaseous carbon dioxide. These CO_2 molecules can diffuse from the silica layer through the silicon oxide/polymer interface into the polymer material. The low-cross-linked polymer material is then oxidized because of complex chemical reactions that change its chemical and physical properties. This means that the silicon oxide/polymer interface gradually moves into the polymer material over time (Fig. 3). The diffusion coefficient of CO_2 in the polymer estimated to be 4.4×10^{-25} m^2 s^{-1} resulted in a shift of the silicon oxide/polymer interface of 35 nm after 27 months.

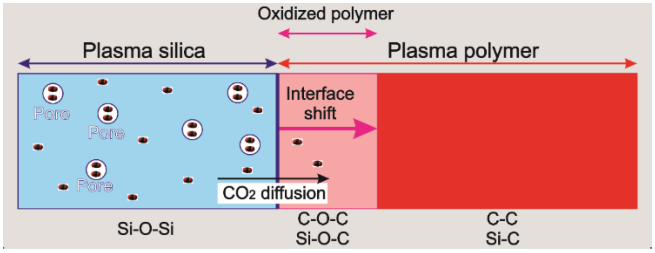

Fig. 3. Schematic view of CO_2 diffusion from glassy silica into a polymer material.

Structural study of the novel superconductor UTe2

Laboratory of Tandetron

Evgenia Chitrova

Proposal ID

565

Structural study of the novel superconductor UTe_2

Evgenia A. Tereshina-Chitrova, O. Koloskova, P. Malinsky, A. Mackova

The recent discovery of unconventional superconductivity in UTe_2 [1] has sparked a keen interest in conducting thorough investigations into compounds with different U to Te ratios. In our work we focused on studying the formation and properties of U-Te thin films with varied composition prepared by the *dc* sputtering technique.

Measurement of Te/U layers was carried out at the ÚJF of the Academy of Sciences of the Czech Republic on a Tandetron 4130 MC tandem accelerator. The samples were measured by the RBS method using a beam of He+ ions with energies of 1.7 and 2.5 MeV to determine the concentration of U and Te on a straight geometry (entry angle 0°, scattering angle 170°) and on an oblique geometry (entry angle 50°, scattering angle 170°). The RBS-Ch method was used to determine single crystal quality, where appropriate. The spectra were evaluated with the software SIMNRA 6.06.

First of all, the RBS study showed that MgO substrates are not appropriate for the samples production at elevated temperatures as both Mg and O diffuse into the thickness of the film. Hence, for the samples production on MgO substrates (very close lattice parameter in MgO with lattice parameter *b* in UTe_2), the substrates have to be cooled to avoid interdiffusion. Second problem revealed by RBS is that thermal sputtering of Te is not suitable for production of homogeneous samples, as from measuring depth profiles of U, Te, and Mg or F we found the concentration gradient in all the samples.

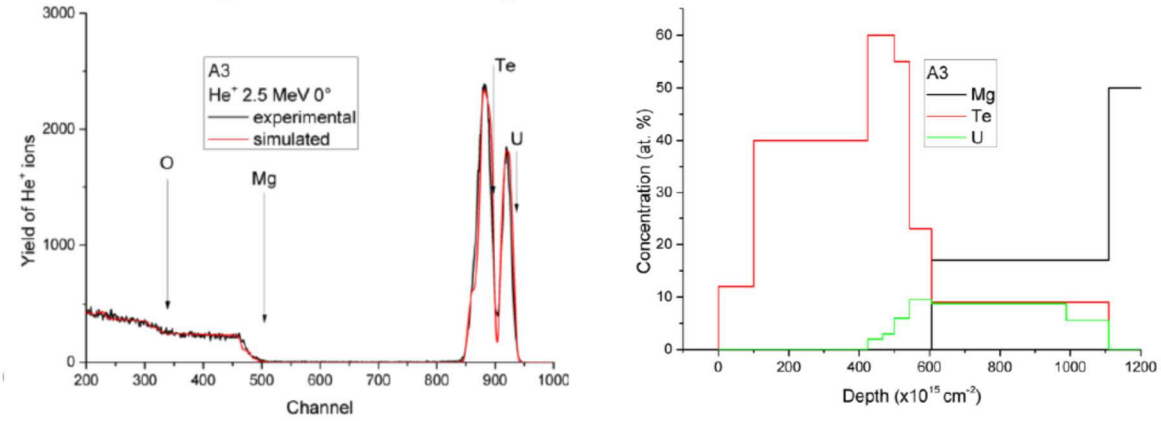

Figure 1: RBS spectra and U and Te depth profiles of sample A3. In addition to U and Te, the presence of other elements (O, C or N) in the layer is assumed, which would had to be verified by further measurements. On the depth profiles of the elements (bottom right) is an obvious surface layer containing Te 0 (400×1015cm-2) and only below it begins a layer containing both Te and U.

Solution for this problem is in constructing a special shape of the sputter source, where uranium and Te first sputter into some (closed) volume and then are released onto the substrate in a controllable manner. We have already prepared a new set of samples, which will be further investigated in our next proposal.

References:

[1] S. Ran et al., Science 365, 684 (2019).

Micro and nano-sized membranes on polyethylene terephthalate realized by ion micro beam

Laboratory of Tandetron

Mariapompea Cutroneo

Proposal ID

568

Report 568

Polymer membranes are conventionally prepared using high-energy particles from radioactive decay or by the bombardment of hundreds of MeVs energy ions. In both circumstances, tracks of damage are produced by particles/ions passing through the polymer, and successively, the damaged material is removed by chemical etching to create narrow pores. This process ensures nanosized pore diameter but with random placement, leading to non-uniform local pore density and low membrane porosity, which is necessary to reduce the risk of their overlapping. The present study is focused on the use of polyethylene terephthalate (PET) foils irradiated by 10.0 MeV carbon ions, easily achievable with ordinary ion accelerators. The ion irradiation conditions and the chemical etching conditions were monitored to obtain customized pore locations without pore overlapping in PET. The quality, shape, and size of the pores generated in the micromembranes can have a large impact on their applicability.

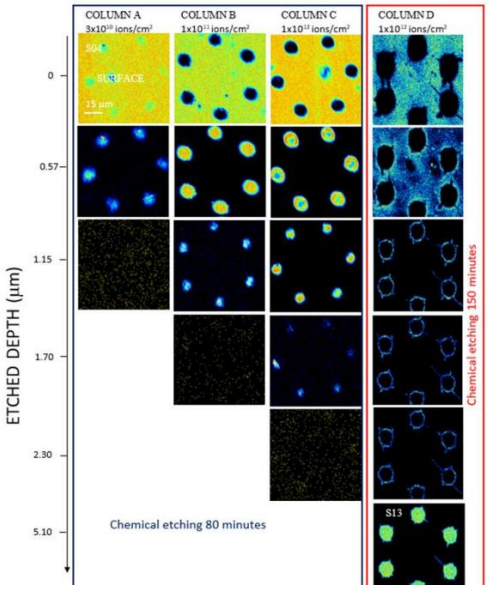

The results indicate that the depth of the pores fabricated on PET foils by ion irradiation progressively increases with the ion fluence and, at the same ion fluence condition, increases with the chemical etching time. **Figure 1** shows the details of the pore edges and the surface morphology of the polymeric foils at 75 μm × 75 μm scan size, considering one pattern as almost representative of the whole membrane.

The Scanning Transmission Ion Microscopy (STIM) coupled with a computer code created in our laboratory was implemented to acquire new visual and quantitative insights on fabricated membranes.

The TrackHH is the code based on the Monte Carlo simulation which is the corrected version of the previous TOM. The modeling of the pore size and shape is obtained through the comparison of the experimental and the simulated energy spectra. The spectra are computed using a very low ion beam divergence and almost 0◦ incidence angle and use the following free parameters: thickness, density, inhomogeneities and structure of the used foil, number of tracks formed in the foil, and pore geometry.

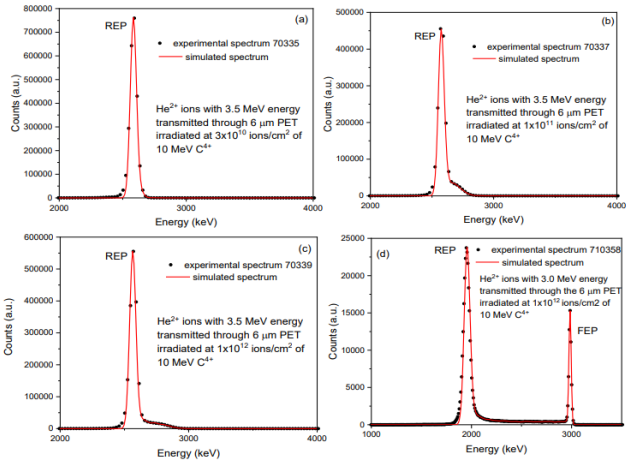

Figure 2. Comparison between the experimental and simulated spectra obtained by TrackHH code for the PET foils irradiated by ions.

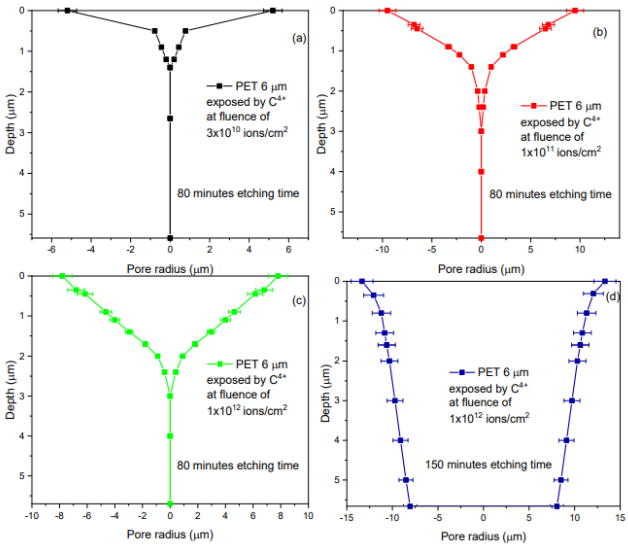

Figure 3. Model of the pores' shape for the membranes

Over the undeniable advantages related to the use of ion lithography processing, the good control of the ion fluence and the high blanking time are crucial for the production of membranes enclosing pores in a chosen pattern. This technique minimizes the merging of the adjacent tracks and promotes the customization of the size and shape of the pores. A Tandetron accelerator, widely available in plenty of laboratories all over the world, was used to deliver carbon ions with an energy of 10 MeV focused by a micro ion beam system on a thin PET foil. The latent tracks formed by ion irradiation of the foils were converted into channels after chemical etching. Conversely, at an ion fluence of 1×10^{12} ions/cm^2 and 150 min etching time, the pores were fully etched and showed a cylindrical shape and diameter of about 20 μm. The joint application of STIM and TrackHH presented congruence in both the formed pore size and the value of the final foil thickness. The relative error in pore size can be estimated at about 10% by direct comparison between the value of the pore diameters evaluated by STIM and TrackHH code.

Modification of graphene and polymer thin films by multi-energy implantation of Cu and Ag ions

Laboratory of Tandetron

Eva Štpanovská

Proposal ID

600

Final report proposal: Modification of graphene and polymer thin films by multi-energy implantation of Cu^+ and Ag^+ ions

As part of the experiments, multi-energy implantation of Cu^+ and Ag^+ ions was performed into multilayer graphene and polymeric materials (PI, PMMA, COC) to modify their properties for potential application in lithium-ion batteries (LIBs).

For graphene, the implantation aimed to mitigate restacking, which reduces active surface area and degrades electrochemical stability. The gradient distribution of metal ions was designed to create electrostatic pillars that maintain layer separation and enable efficient lithium-ion transport. **Figure 1 presents the Raman spectra of graphene after Cu^+ implantation, showing an increase in sp^2 bond intensity and the 2D peak, indicating preserved conductivity while modifying interlayer interactions.**

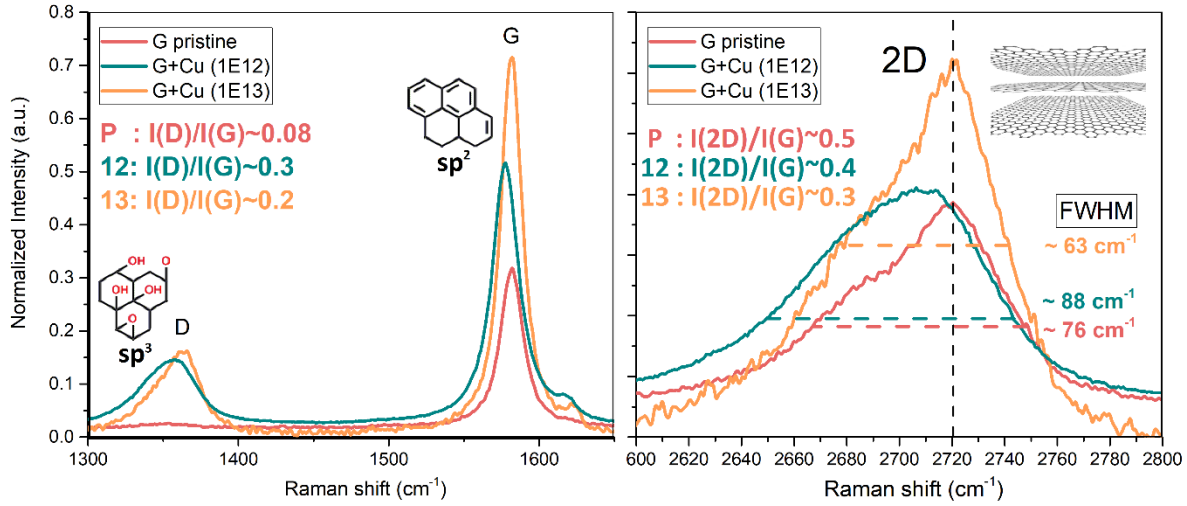

Figure 1 Raman spectra of multilayer graphene before and after Cu^+ ion implantation at fluences of 1×10^{12} cm^{-2} and 1×10^{13} cm^{-2}. The increase in the D band intensity (I(D)/I(G)) indicates defect formation, while the 2D band remains prominent, suggesting preserved sp^2 domains. The narrowing of the 2D peak (FWHM) with fluence suggests modifications in interlayer interactions, potentially reducing restacking effects.

For polymers, implantation focused on enhancing dielectric and mechanical properties. PI was modified to improve polarizability and adhesion, PMMA to enhance ionic conductivity through interactions between implanted ions and carbonyl groups, and COC was investigated as a potential protective layer for SEI stabilization. The multi-energy approach ensured a gradual modification from the surface to the bulk, with low fluences inducing minor structural changes and higher fluences promoting conductive pathways and polymer cross-linking.

[1] Adenusi, H., et al. (2023). Lithium Batteries and the Solid Electrolyte Interphase (SEI)—Progress and Outlook. In Advanced Energy Materials (Vol. 13, Issue 10). Wiley.
[2] An, S. J., et al. (2016). The state of understanding of the lithium-ion-battery graphite solid electrolyte interphase (SEI) and its relationship to formation cycling. In Carbon
[3] Shen, Y., et al. (2021). Achieving Desirable Initial Coulombic Efficiencies and Full Capacity Utilization of Li?Ion Batteries by Chemical Prelithiation of Graphite Anode.

Ni4(Nb,W,Ti)2O9 corundum like-compounds: cationic distribution and magnetic structure.

Neutron Physics Laboratory - Neutron diffraction

Christine Martin

Proposal ID

569

Report regarding the proposal "$Ni_4(Nb,W,Ti)_2O_9$ corundum like-compounds: cationic distribution and magnetic structure." by C. Martin *et al.*

Neutron powder diffraction was performed using the MEREDIT diffractometer at room temperature, 55 K and 15 K, for two samples corresponding to x = 0.05 and x = 0.1 in the $Ni_4Nb^{5+}_{2-x}Ti^{4+}_xW^{6+}_xO_9$ formula.

The results are described below for the x=0.1 sample.
The RT NPD pattern is characteristic of the expected large *Fdd2* cell (*a* = 28.568 Å, *b* = 10.091Å and *c* = 17.538 Å). A very small amount of NiO is also observed. The refinement of the structure, also using the synchrotron diffraction data obtained in ALBA (Spain), is in progress. Indeed, the calculations are rather delicate since the structure corresponds to 18 oxygen positions, 10 nickel positions and 4 niobium positions, on these 32 sites, only 4 are not general, and mixed occupations have to be introduced to distribute Ti and W (on Nb sites probably). Moreover, some peaks of the SXRPD patterns are broadened compared to the others, probably in link with some disorder due to the mixing of the cations. In addition, transmission electron microscopy is also in progress to confirm (or not) the space group and the metric, to have information on the cationic distribution and on the existence of structural defects.
The *figure 1* shows the beginning of this structural refinement work with the starting patterns (in combined mode, by using Fullprof software).

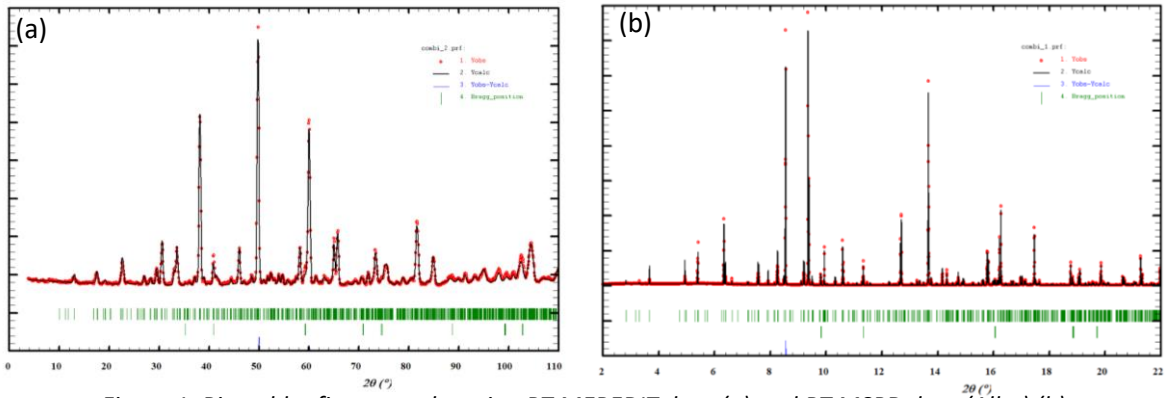

Figure 1: Rietveld refinements by using RT MEREDIT data (a) and RT MSPD data (Alba) (b).

The temperature dependence of the NPD patterns, shown in *figure 2a*, is in agreement with the magnetic properties, illustrated in *figures 2a and b*: magnetic peaks are observed at 55 K and 15 K (highlighted by vertical orange arrows) those relative intensities are varying in between both low temperature patterns.

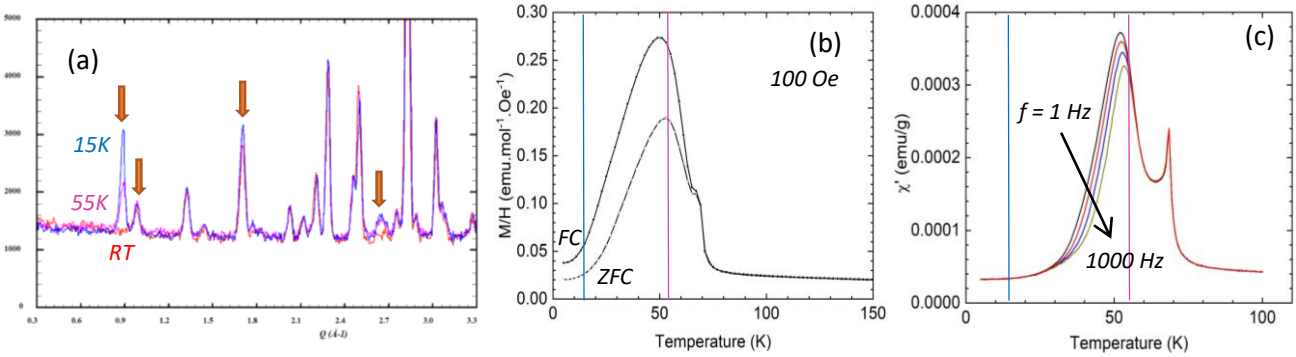

Figure 2: (a) NPD patterns of $Ni_4Nb_{1.8}Ti_{0.1}W_{0.1}O_9$ recorded at RT (red), 55 K (pink) and 15 K (blue); temperature dependence of the magnetic susceptibility: dc, zero field cooling and field cooling modes (b) and ac using 4 frequencies (c).

The analysis of these data is clearly in its early stages. Nevertheless, the preliminary tests using the *Fd'd'2* and *Fd'd2'* magnetic space groups, and same magnetic and crystallographic cells, are promising.

Since the x = 0.05 compound corresponds to a mixture of two close phases, i.e. the large *Fdd2* one and the parent small *Pbcn* one, these data will be used to understand the moving from one structure to the other one and to identify the origin of the super structure.

Macroporous PDMS decorated with organic and inorganic materials for application in microelectronics

Laboratory of Tandetron

Mariapompea Cutroneo

Proposal ID

473

Report

A hybrid material incorporating gold nanoparticles (Au-NPs) in polydimethylsiloxane (PDMS) has been synthesized. Gold nanoparticles gained wide interest for their optical, chemical and physical properties, such as surface plasmon oscillations resonant absorption, chemical structure, imaging and sensing. Au-NPs can be conjugated with several functionalizing agents, such as polymeric chains, improving their properties and performances. PDMS composites with weight percentages ranging between 0.1 and 0.2% of spherical Au-NPs (10 nm diameter), were produced. The surface morphology was investigated by atomic force microscopy (AFM) and wetting ability analyses see **Figure 2**.

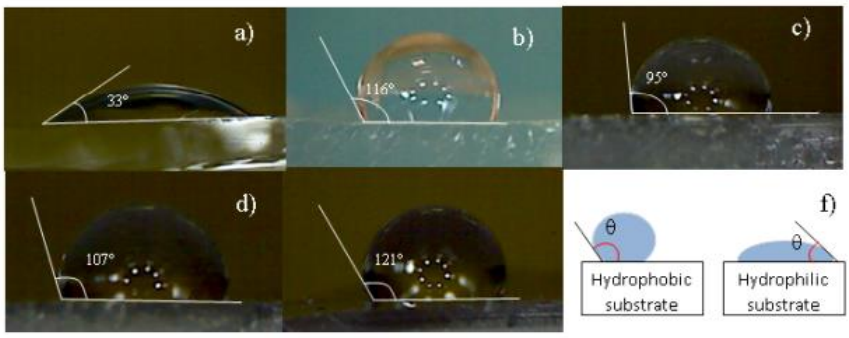

Figure 2. *Optical images for wettability measurements of virgin Glass (a), virgin PDMS (b), PDMS containing 0.1% wt NPs (c) PDMS containing 0.2% wt wet Au-NPs (d) PDMS containing 0.2% wt dried Au-NPs (e) and schematic representation of water molecules on different substrates (d).*

The presence of structures inside both virgin and hybrid PDMS containing Au-NPs was preliminary investigated by Small Angle X-ray Scattering (SAXS). The optical performance of such hybrid material was studied by UV-VIS spectroscopy, in transmission mode.

Polymers containing metal nanoparticles have gained high interest in the optical field, due to their special optical properties, such as dichroism, switching and controlled absorption coefficient. The optical responses of Au-NPs embedded in PDMS films are connected to the Au-NPs features, which result from the adopted method. The PDMS network, does not protect the gold nanoparticles from aggregation as observed in the present study. The changes in the morphological and optical properties of the matrix are related to the presence of the Au-NPs dopants in PDMS working as links uniformly distributed in the polymer. The appearance of pink and violet PDMS-AuNPs composites suggests the presence of Au-NPs aggregates with different size, as confirmed by SAXS and AFM analyses and optical microscopy.

The UV-Vis measurement shows the maximum peak absorption at around 517 nm–528 nm indicating Au-NPs with size ranging between 10 nm and 60 nm in the investigated samples.

The sample exhibiting higher absorption is the PDMS containing 0.2 wt% of Au-NPs due to less aggregation of the fillers and consequent higher number of NPs per volume of matrix. The presence of Au NPs in PDMS improves the absorbance of the matrix as observed also during the laser irradiation of the sample leading to the enhancement of the emitted ion energy, electron density and plasma temperature. It is established that the higher the size of Au NPs is the higher the temperature in the surrounding area and the longer the time to reach the thermal equilibrium. Work is in progress to investigate the thermal behaviour of the PDMS containing Au-NPs, which is crucial for the control of the temperature distribution for applications in metallic micro- and nano-fabrication process by direct laser writing and ion beam writing but also for material growth, material absorption control, cancer treatment and controlled drug release.

Publications:

[1] Cutroneo M.; Havranek V.; Mackova A.; Malinsky P.; Silipigni L.; Slepicka P.; Fajstavr D.; Torrisi L., Synthesis of porous polydimethylsiloxane gold nanoparticles composites by a single step laser ablation process, International Journal of Molecular Sciences 2021

[2] Cutroneo, M.; Havránek, V.; Semián, V.; Torrisi, A.; Macková, A.; Malinský, P.; Silipigni, L.; Slepička, P.; Fajstavr, D.; Torrisi, L. (2021) Porous polydimethylsiloxane filled with graphene-based material for biomedicine. Journal of Porous Materials. 28, 1481-1491.

[3] Cutroneo, M.; Havránek, V.; Macková, A.; Malinský, P.; Torrisi, A.; Silipigni, L.; Slepička, P.; Fajstavr, D.; Torrisi, L. (2021) The characterisation of polydimethylsiloxane containing gold nanoparticles as a function of curing time. Surface and Interface Analysis. 53(7), 618-626. doi: 10.1002/sia.6948

[4] Cutroneo, M.; Havránek, V.; Torrisi, A.; Macková, A.; Malinský, P.; Slepička, P.; Sofer, Z.; Torrisi, L. (2020) Polydimethylsiloxane-graphene oxide composite improving performance by ion beam irradiation. *Surface and Interface Analysis. 52*(12), 1156-1162. doi: 10.1002/sia.6882

Interface characterization of Li metal / Lipon batteries

Neutron Physics Laboratory - Nuclear analytical methods with neutrons

Ralph Gilles

Proposal ID

573

Report regarding proposal ID 573: “Interface characterization of Li metal / Lipon batteries”

Ralph Gilles, Technical University of Munich (TUM), Germany
Andrew Westover, Katie Browning, Oak Ridge National Lab, USA
Antonino Cannavo, Jiri Vacik, G. Ceccio, Nuclear Physics Institute in Rez, Czech Republic

The experiments were carried out with the NDP spectrometer at the Nuclear Physics Institute (NPI) in Rez, Czech Republic, which is a part of the Center of Accelerators and Nuclear Analytical Methods (CANAM). The performed experiment deals with the study of interface between Li metal and Lipon layer to understand better the interface between the solid electrolyte Lipon and Li metal. Previous experiments show the problem of oxidation if Li metal layer was on top of the Lipon layer. Two strategies were followed to overcome this problem. First, the stacking sequence was changed that Lipon was on top and Li metal below as Lipon is less reactive with air than Li metal. To understand better the interface of Li metal and Lipon, an artificial layer was implemented between the two layers to split better the single signals from Li metal and Lipon. The idea was to use single layer information to understand better the interface region of Li metal and Lipon. In addition, AFM measurements were carried out to observe if surface oxidation occurs (due to oxidation, there is a significant increase in surface roughness, from which the degree of surface oxidation can be inferred).

The focus was on two kind of sample sets. First stack consists of i. Li~400 nm ii. Ni–50 nm, iii. Lipon-100 nm and the substrate sapphire -1 mm. The second stack is layered with i. Li~400 nm, Ni-50 nm and iii. Lipon-500 nm and sapphire -1mm.

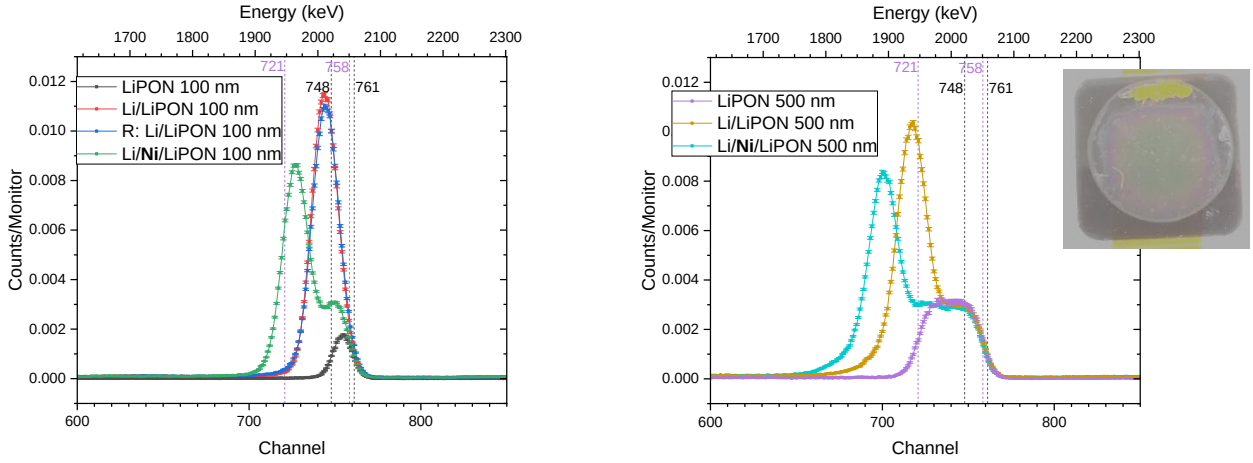

Fig. 1 The layer stacks with different Lipon thickness of 100 nm and 500 nm are compared with NDP measurements showing the influence of Ni interlayer and Lipon on Li metal layer. AFM image proofs no oxidation on the surface.

First results confirm the expected Lipon thickness of 448 nm (500 nm) and 95 nm (100 nm) assuming an atomic density of 7.81 x 10^{22} [at./cm^3] for Lipon. The Lipon layer on the top and Li below avoid the oxidation on the surface proofed with AFM technique. A mixed layer for the Li metal / Lipon stack was detected but a first fitting model for the Li metal / Ni / Lipon stack failed as Li diffusion takes place in the Ni layer. An exchange of the Ni layer with another metal with higher stability against Li diffusion could help to distinguish better the influence of single layer Li metal and Lipon using NDP in comparison to the bilayer Li metal / Lipon.

Using neutron diffraction to characterize bulk texture in additively manufactured magnesium alloy

Neutron Physics Laboratory - Neutron diffraction

Lisa Larsson

Proposal ID

574

Report regarding proposal "Using neutron diffraction to characterize bulk texture in additively manufactured magnesium alloy"

Additive manufacturing by powder bed fusion laser beam (PBF-LB) has opened up new possibilities in the manufacturing of biodegradable magnesium (Mg) alloys. Due to the unique thermal history of the process, the resulting part typically present anisotropic properties and texture. In terms of mechanical properties, the build direction does have a large impact on the final WE43 alloy specimens (Fig. 1). The laser scan strategy slightly alters alloy microstructure, but only has a minor effect on the mechanical response of the Mg-parts, which is in contrast to other metals manufactured by PBF-LB (e.g. [3]). We hypothesized this to be due to changes resulting grain orientations and texture in the direction of loading when it comes to the effect of build direction, and limited grain growth between layers minimizing the effect of scan strategy on resulting properties.

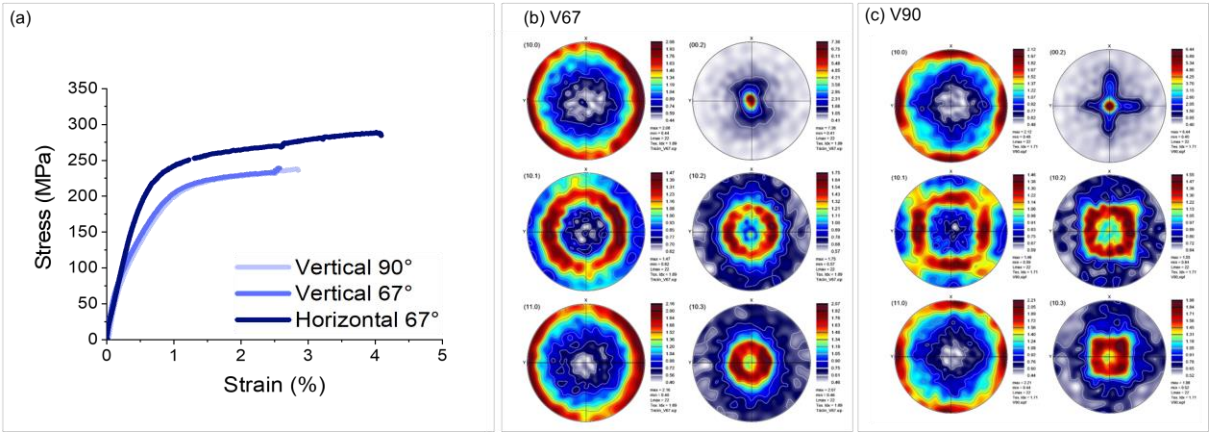

Figure 1. (a) Stress-strain curve for horizontally built samples and vertically built samples, and two different scan strategies. (b) Calculated neutron pole figures showing preferential crystallographic grain orientations, for the vertically printed samples when the scanning vectors are rotated 67°, and (c) 90° degrees between each scanned layer.

To determine the bulk texture of the as-printed components (Figure 1a), neutron diffraction was used to measure a large sample volume of 10 mm diameter cylinders. This ensures that observations are representative of the whole sample. Samples were fixed on the Euler goniometer and rotated along φ (0–360°) and χ (0–90°) angles with a step of 5°. Variation of neutron diffracted intensities for 6 individual reflections [(100), (002), (101), (102), (110) and (103)] were collected for each orientation on the MEREDIT instrument, using a neutron wavelength of 1.46 Å. The data was analysed using ATEX software. The orientation distribution function (ODF) was calculated for each sample, and pole figures for predefined reflections were calculated for easy comparison of all samples.

Some of the pole figures calculated from the neutron diffraction measurements are presented in Figure 1b and 1c. The sample printed with a 67°-rotation scan rotation shows higher intensity with more pronounced basal texture (i.e. a fiber texture with strong "out of plane" texture along the c-axis but no "in-plane" texture). For the sample printed with 90° rotation between layers it is observed that it is affecting also the "in-plane" texture. A cross-like pattern is observed for the (002)-pole and a square-like pattern for the (101)-pole, which relates to the 90° pattern that the laser shifts between layers. The degree of texture is, however, much smaller in-plane than out of plane. These results show the possibility of tuning both in-plane and out of plane texture by controlling sample orientation and scan strategy for LPBF of Mg alloy WE43. A more detailed analysis of how solidification and grain growth is influenced by the laser scanning pattern is currently being performed and a possible future experimental proposal.

References

[1] Jithin James Marattukalam et al., 2022. Materials Design. The effect of laser scanning strategies on texture, mechanical properties, and site-specific grain orientation in selective laser melted 316L SS

Neutron Depth Profile Measurements to Determine the Influence of Tin Coating on the Lithium Distribu

Neutron Physics Laboratory - Nuclear analytical methods with neutrons

Pham Thien An

Proposal ID

578

Report regarding: “Neutron Depth Profile Measurements to Determine the Influence of Tin Coating on the Lithium Distribution of Aluminium Electrodes”

THIEN AN PHAM[1,2], LUKE WELLS[3], VACÍK JIŘÍ[4], RALPH GILLES[1]

[1]*Heinz Maier-Leibnitz Zentrum (MLZ), TU München, Lichtenbergstr. 1, 85748 Garching, Germany*
[2]*TU München, Physik-Department, LS Funktionelle Materialien, James-Franck-Str. 1, 85748 Garching, Germany*
[3]*RTWH Aachen, Institut für Stromrichtertechnik und Elektrische Antriebe, Jägerstr. 17-19, 52066 Aachen, Germany*
[4]*Nuclear Physics Institute of the Czech Academy of Sciences, Husinec - Řež, čp. 130, 250 68 Řež, Czech Republic*

Al electrodes were with a Sn layer to prevent the parasitic reaction between Al and the electrolyte. The impact of the Sn coating should have been measured with neutron depth profiling by comparing neat and coated samples.

The initial plan was the measurement of the Al electrodes after multiple cycles at different states of charge. However, the degradation of the samples was more substantial than expected. As a result, we have observed the pulverization of the electrodes, which made them both difficult to transport and impossible to collect usable information regarding the concentration and depth. The determination of a Li depth profile was not possible that way. In Figure 1, all the samples are shown. Sample 1, the uncoated pristine aluminium containing no Li, is the only sample that has shown no pulverization as expected.

The measurements were stopped after the first sample since the samples could not be measured in the state that they were in. Due to difficulties in preparing more stable Sn-coated samples from our sample provider, no further measurements are planned soon.

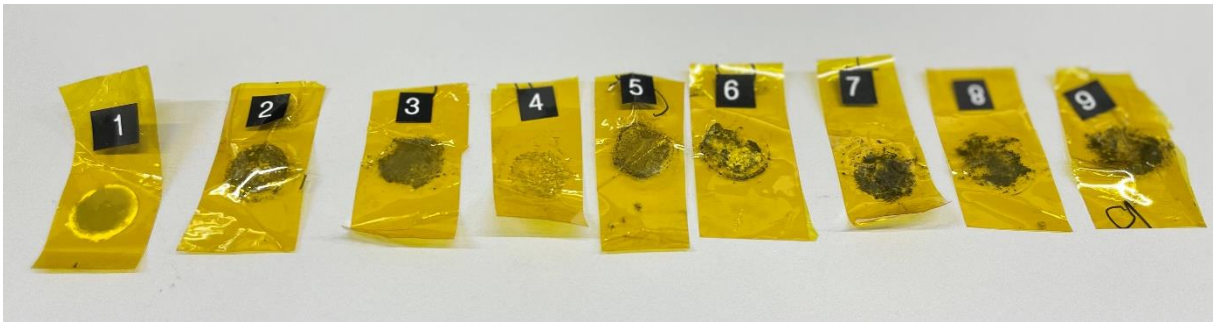

Figure 1: Photo of the prepared Sn-coated aluminium electrodes. The pulverization is clearly visible in all the samples (number 2-9).The uncoated pristine aluminium electrode (number 1) is the only sample in a solid state.

Study of elemental composition of volcanic ashes for geopolymer applications

Laboratory of Tandetron

Giovanni Ceccio

Proposal ID

546

Report - Proposal 546 “Study of elemental composition of volcanic ashes for geopolymer applications”

The project was focused on the determination of elemental composition of several volcanic ashes by nuclear analytical techniques such as RBS and Ion Microprobe-IBA using MeV ions (from Tandetron accelerator).

a) b)

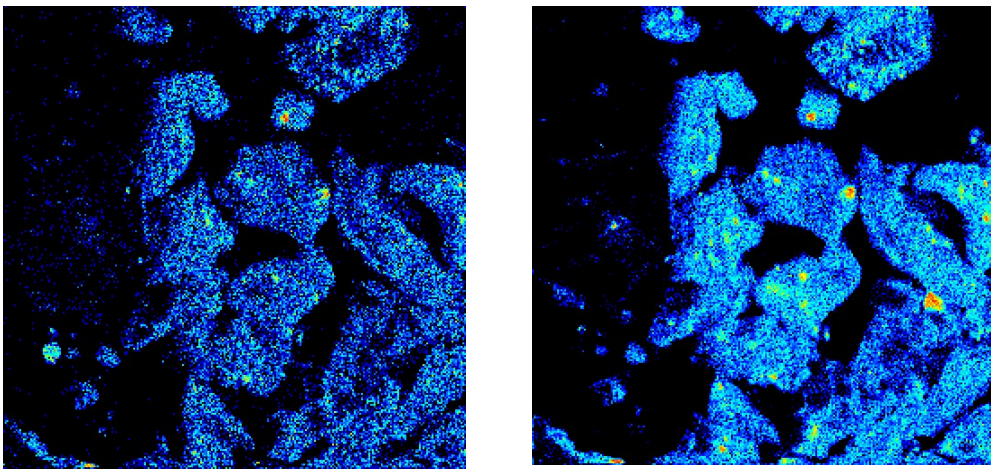

c) d)

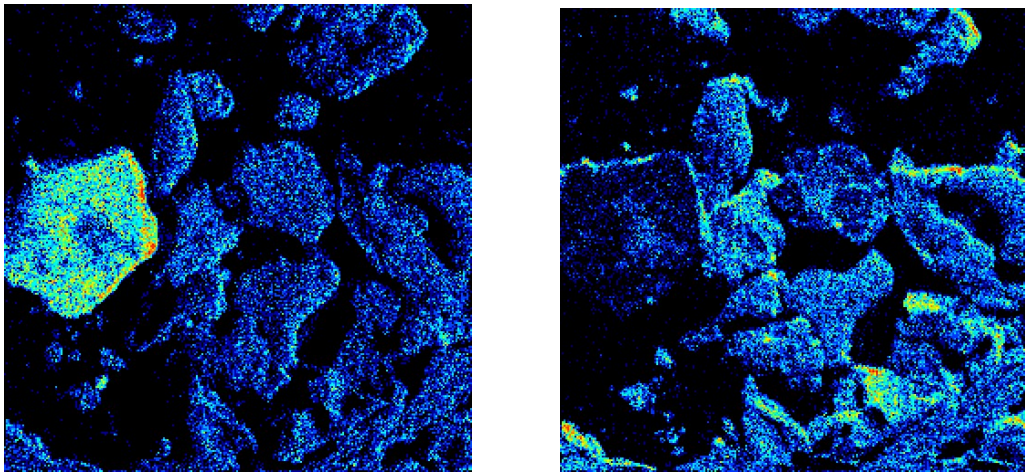

Microbeam analysis of volcano ashes, elemental investigation of: a) Ti, b) Fe, c) Si and d) Al

The obtained data are currently under evaluation and the comparison with complementary techniques suggests the possibility to have small traces of particular elements suitable for the preparation of geopolymers. The results are suitable for future publications when the data evaluation will be completed.

Impact of compressive stress on the low-symmetry phases of Ni-Mn-Ga-Fe magnetic shape memory alloys

Neutron Physics Laboratory - Neutron diffraction

Milan Klicpera

Proposal ID

579

Experimental report

Experiment title:
Impact of compressive stress on the low-symmetry phases of Ni-Mn-Ga-Fe magnetic shape memory alloys

Instrument:
Strain Diffractometer TKSN-400

Experimental team:
Milan Klicpera, Charles University, Faculty of Mathematics and Physics.
Petr Veřtát, Academy of Sciences of the Czech Republic, Institute of Physics

Local contact:
Gergely Farkaš

Experimental details:
We performed a neutron diffraction experiment on modulation satellite positions for the five-layered modulated (10M) martensites of the Ni-Mn-Ga-Fe single crystal under compressive stress. The experiment was pioneering research on the influence of (quasi-)uniaxial pressure on the modulated martensitic phase, testing the feasibility of our approaches/hypotheses using instrumentation of CANAM.

The studied single crystal was aligned, its quality verified, and reflections (220) and (400) were found. Subsequently, it was inserted into the stress device and the alignment was checked again. A series of scans of the reciprocal space were performed to follow the line between the two reflections. Modulation satellites were observed, and their positions were identified. Finally, the evolution of the satellite positions with applied stress was followed.

The experiment allowed us:
(1) to verify the good quality of the investigated single crystal.
(2) to prove that the instrument and technique are feasible for in-situ investigations of Ni-Mn-Ga materials.
(3) to inspect the positions of modulation satellites (see Fig.1 as an example).
(4) to follow the evolution of satellites with applied stress and calculate the modulation q-vector.

Considering the success of performed experiment, further (continuation) experiments will be proposed in near future. Other directions of reciprocal space are to be mapped and new compositions with 10M phase are to be studied.

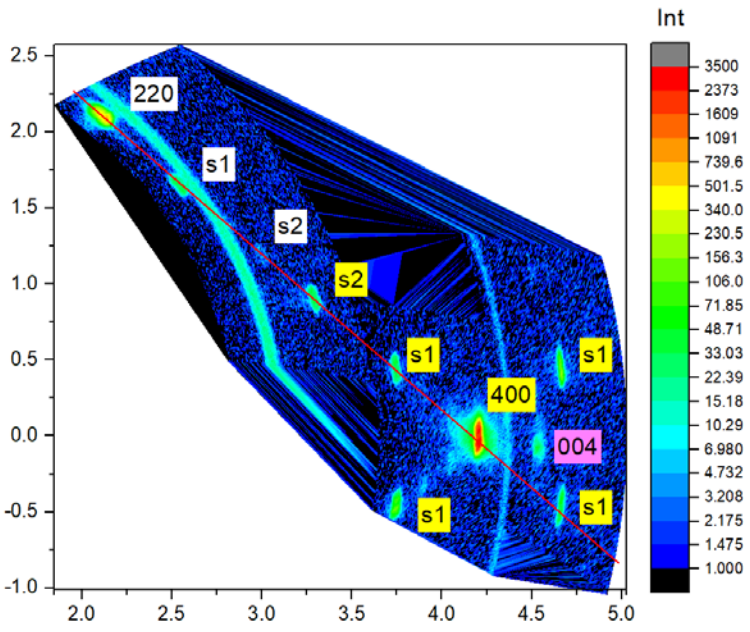

Fig.1 – map of reciprocal space created by convoluting several qx-qy scans. Reflections (220) and (400) and satelittes between them are marked. Parasitic (004) reflection (from other martensitic phase) is marked as well.

Controlled fabrication of self-assembled iron-fullerene nanocomposite films

Laboratory of Tandetron

Vasyl Lavrentiev

Proposal ID

582

Project title: **Controlled fabrication of self-assembled iron-fullerene nanocomposite films**

Researcher: **Vasily Lavrentiev**

Affiliation: *Nuclear Physics Institute CAS, Rez-130, Husinec, 250 68*

Project term: *1.4.2023-1.1.2024* (proposal 582)

By implementing this cycle of the experiments, the goal of the project was achieved, namely, (1) the obtained results evidence successful creation of the Fe-C_{60} nanocomposite (NC) films through self-assembly phenomenon, and secondly, (2) stability of the Fe-C_{60} structure and composition upon keeping the films in an ambient air was verified. The required information has been obtained using Rutherford backscattering spectrometry (RBS) and atomic force microscopy (AFM) techniques. The Fe-C_{60} NC films have been fabricated through simultaneous deposition of Fe and C_{60} on Si(100) using physical vapor deposition technique. 1). According to our previous results, the applied deposition setup should lead to formation of nanocomposite nanostructure as a uniform ensemble of the Fe nanoparticles (NPs) immersed in the C_{60} medium [1, 2]. Formation of such a specific nanostructure is confirmed by analysis of the RBS spectra, some of which are shown in *Figure 1a*. Except the anticipated Fe and C components, the RBS spectra also include the ion scattering effect from oxygen at the deposited layers, which, evidently, was introduced during the sample transfer to the RBS chamber (the ion-beam experiments are in *ex-situ* conditions). Analysis of the correlations between the Fe and O contents in the deposited samples implies the formation of the oxidized Fe NPs [1]. 2). *Figure 1b* demonstrates the RBS spectra recorded from the $Fe_xO_yC_{60}$ films with $x \approx 12$ recorded from the samples kept at the ambient air during different time. The RBS spectra show only slight change revealing some increase in the O content at the longer air exposure. At the same time, AFM does not distinguish serious changes in the surface topography after the air exposure (see *Figure 1c*).

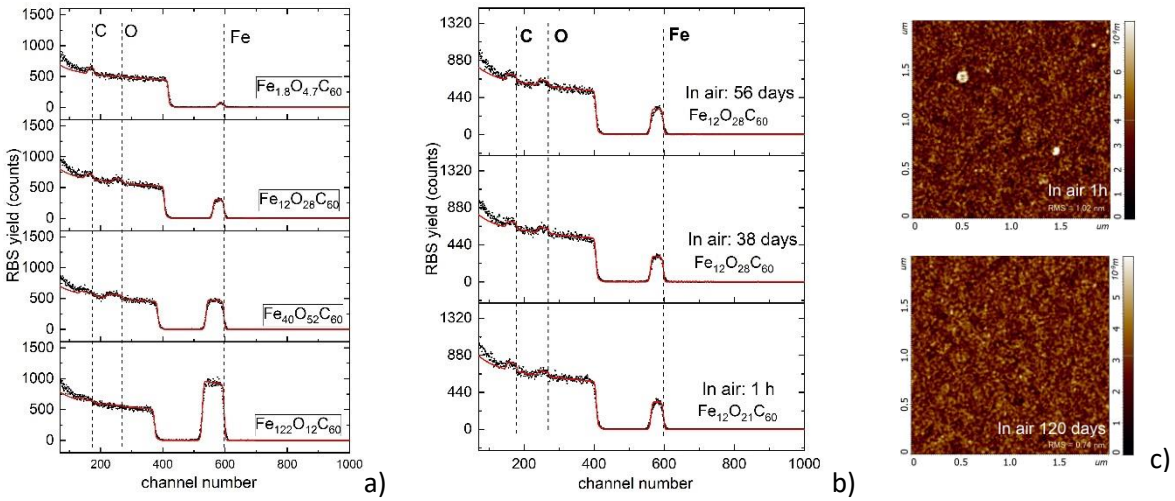

Figure 1. **(a)** The experimental (black dots) and simulated (red lines) RBS spectra of the as-deposited $Fe_x(O_y)C_{60}$ films with different Fe content. **(b)** The RBS spectra of the $Fe_x(O_y)C_{60}$ film with $x \approx 12$ recorded after the different times of the sample air exposure. **(c)** AFM images of the surface of the film with $x=12$ as-deposited (top image) and after the air exposure for 120 days (bottom image).

The results obtained within this project will be published soon in some international journals.

References

1. V. Lavrentiev et al. Carbon 103 (2016) 425.
2. V. Lavrentiev et al. Carbon 184 (2021) 34.

Neutron depth profiling for understanding the impact of Li-excess in Ni-rich layered NMC cathodes fo

Neutron Physics Laboratory - Nuclear analytical methods with neutrons

Pham Thien An

Proposal ID

551

Report regarding: “Neutron depth profiling for understanding the impact of Li-excess in Ni-rich layered NMC cathodes for long-term battery operation”

THIEN AN PHAM[1,2], AHMAD OMAR [3], DARIA MIKHAILOVA[3], VACÍK JIŘÍ[4], RALPH GILLES[1]

[1]Heinz Maier-Leibnitz Zentrum (MLZ), TU München, Lichtenbergstr. 1, 85748 Garching, Germany
[2]TU München, Physik-Department, LS Funktionelle Materialien, James-Franck-Str. 1, 85748 Garching, Germany
[3]Leibniz Institute for Solid State and Materials Research Dresden, Helmholtzstraße 20, 01069 Dresden, Germany
[4]Nuclear Physics Institute of the Czech Academy of Sciences, Husinec - Řež, čp. 130, 250 68 Řež, Czech Republic

Ni-rich electrode materials should have been investigated using the neutron depth profiling method. For that, samples of different compositions in pristine state and after ten charge-discharge cycles were prepared. The samples were sealed in kapton foil to prevent degradation as the Li is very reactive, and the composition of the samples could change when in contact with ambient air. Unfortunately, the thickness of the used foils was too high; therefore, the signal from the samples was too low to retrieve more information.

Figure 1 shows the difference between a pristine sample and one cycled for ten cycles. Here, the difference between the counts per second was minuscule despite the long measuring time, which can be attributed to the absorption of the kapton foil.

Unfortunately, the measurements were conducted right at the end of the project period, and thus, there were no remaining funds to start another campaign to prepare a new batch of samples. Therefore, this measurement was stopped.

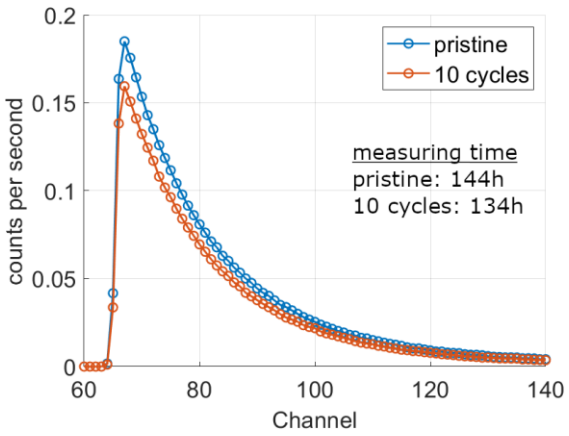

Figure 1: NDP spectra for a pristine and a cylced electrode.

Localisation of the stresses in Mg alloy during twinning and detwinning process - part 2

Neutron Physics Laboratory - Neutron diffraction

Marcin Wronski

Proposal ID

585

Report regarding proposal "Localisation of the stresses in Mg alloy during twinning and detwinning process - part 2"

M. Wroński P. Kot, A. Baczmański, A. Ludwik, S. Wroński and G. Farkas

The aim of the experiment was to investigate the evolution of lattice strain of magnesium alloy (AZ31) during cycling loading: compression in rolling direction (RD) followed by tensile in RD. Two mechanisms characteristics for hexagonal metals were study: twinning (dominant in compression loading in RD) and de-twinning (dominant in tensile test of pre-compressed sample in RD). Our methodology allows to determine the CRSS values both for twinning as well as for detwinning process.

The initial samples of cylindrical shape with mounting screws were cut along rolling direction (RD) -see Fig 1a.

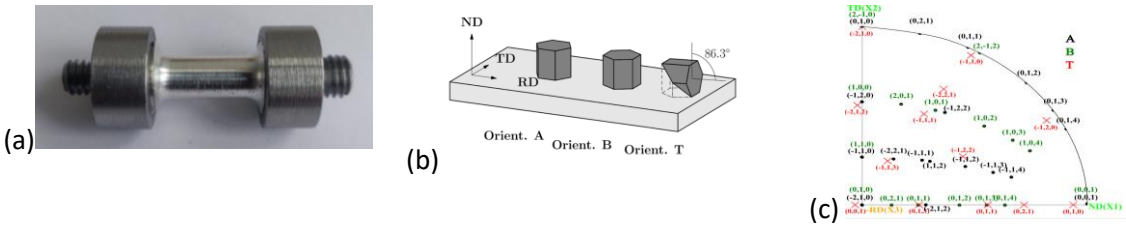

Fig. 1 (a)Project of sample (AZ31) and pistons used in experiments, (b) Visualization of orientations (A, B and T) examined during experiment (c) Poles for orientation A, B and T for which the lattice strains were measured during *in situ* cycling loading in RD. The load is in the center of pole figure.

To perform lattice strains measurements for the selected orientations A, B and T (see Fig. 1b), the tensile rig was mounted in the Eulerian cradle. Poles for which the measurement were performed were presented in Fig. 1c. The measurement was performed for the initial material and after deformation of the sample during cyclic loading test. Lattice strain was measure for different value of external stresses (see Fig. 2a). Strains were measured in 31 directions of scattering vector. Acquisition time for each point was equal to ~16 hours.

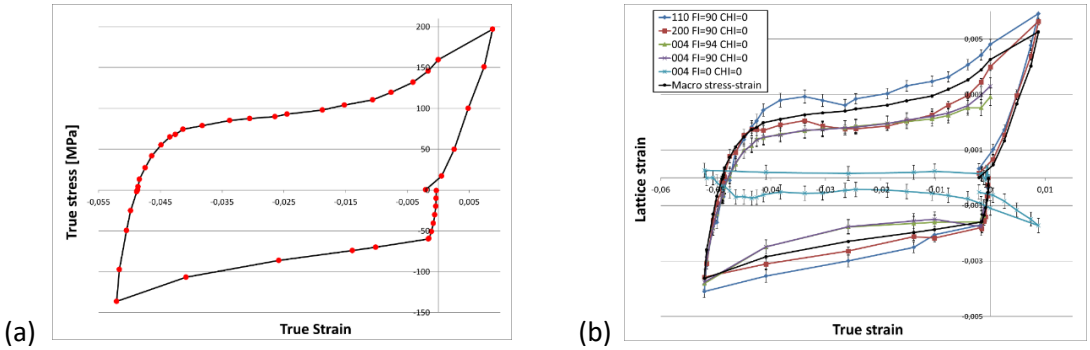

Fig. 5 (a)Stress - strain responses for cyclic loading test in RD direction. Measurement points (neutron diffraction measurements) were marked using red dots. (b) Lattice strains measured in the different direction of scattering vector and macroscopic stress-strain plot for the cyclic loading test in the RD. The error bars correspond to standard uncertainties of measured lattice strains.

Conclusion

In the case of magnesium AZ31 alloy subjected to cyclic loading in RD:

- Twinning and de-twinning mechanism were observed in Mg-alloy deformed along cyclic loading: RDC (rolling direction compression) followed by RDT (rolling direction tension),
- Experimental result allows to determine the RSS and the stress localised at A and B orientation (parent grain orientation) as well at the T-twin orientation during cyclic loading,
- The CRSS values with uncertainties both for twinning as well as for de-twinning process will be estimate. The obtained values will be validated using the elastic-plastic self-consistent model.

Site preferences in machine learning predicted compositionally complex laves phases

Neutron Physics Laboratory - Neutron diffraction

Rebecca Clulow

Proposal ID

586

Report regarding proposal “An investigation into elemental site preferences in a machine-learning predicted compositionally complex Laves-type intermetallic”

V. Enblom, R. Clulow, M. Sahlberg, Uppsala University, Sweden

AB_2 Laves phase intermetallic alloys have been widely studied for their potential in hydrogen storage and compression due to their efficient hydrogen sorption kinetics and long cycling stability. These alloys are typically characterised by larger and smaller elements occupying the A and B sites, respectively, with an atomic radius ratio typically around r_A/r_B=1.225. For hydrogen storage applications, the A-site is often occupied by hydride-forming elements like Ti, Zr, Rare Earth Metals, or Mg, while non-hydride-forming elements such as Fe, Cr, Ni, and Mn generally prefer the B-site. However, certain elements, like V, can display a less definitive site preference, influenced more substantially by factors like temperature or composition.

Recently, our collaborators developed a machine-learning model that predicted a novel composition for hydrogen fuel-cell vehicles: $Ti(V_{0.5}Zr_{0.5})CrMnFeNi$, or more generally written $(Ti_{0.5}V_{0.25}Zr_{0.25})(Cr_{0.25}Mn_{0.25}Fe_{0.25}Ni_{0.25})_2$. This compound is expected to crystallise in the Laves phase C14 ($P6_3/mmc$). Interestingly, V is predicted to occupy the A-site entirely, despite it typically showing a preference towards the B-site in Zr- and Ti-based Laves phases.[1]

With the motivation to investigate site preferences of constituent elements in the predicted compound, with a particular focus on V, a neutron powder diffraction experiment was performed at room temperature using the MEREDIT instrument. This experiment complemented previous X-ray diffraction experiments with CuKα and CuKβ radiation, to gain contrast between all elements.

The data is still under evaluation, but preliminary analysis suggests the existence of a second C14 phase in addition to the previously observed phase, with a slight difference in stoichiometry. Observed and calculated neutron powder diffraction profile is shown in Figure 1. The finding is supported by EDS mapping results.

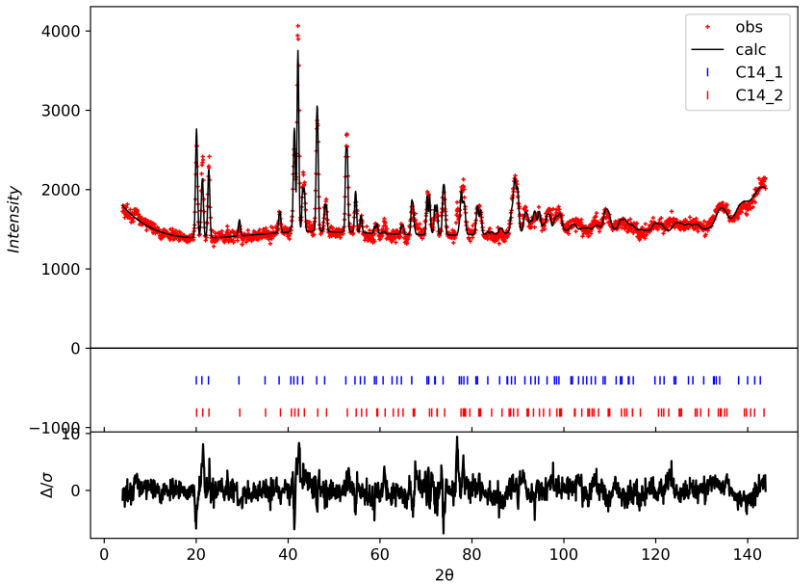

Figure 1. Neutron diffraction profile at 298 K.

References

[1] A. Züttel, D. Chartouni, K. Gross, M. Bächler, and L. Schlapbach, “Structural- and hydriding-properties of the Zr(V0.25Ni0.75)α (1≤α≤4) alloy system,” J Alloys Compd, vol. 253–254, pp. 587–589, 1997, doi: https://doi.org/10.1016/S0925-8388(96)02989-1.